Effect of target material on electrical properties of a two-electrode dielectric barrier helium plasma jet

Nikola Škoro[1], Kinga Kutasi[2], Marija Puač[1], Zoran Lj. Petrović[3,4] and Nevena Puač[1]

[1] Institute of Physics, University of Belgrade, Pregrevica 118, 11080 Belgrade, Serbia
[2] HUN-REN Wigner Research Centre for Physics, Konkoly-Thege Miklós út 29-33, 1525 Budapest, Hungary
[3] Serbian Academy of Sciences and Arts, Knez Mihailova 35, 11000 Belgrade, Serbia
[4] School of Engineering, Ulster University, Jordanstown, Co., Antrim BT37 0QB, UK

E-mail: nskoro@ipb.ac.rs

Abstract

In this paper we present electrical characterization of a dielectric barrier discharge (DBD) plasma jet operating with He (2 slm and 3 slm) as working gas and interacting with Cu, PET and distilled H_2O targets. We used a plasma jet with two copper electrodes wrapped around a glass tube. One electrode was powered by a high-voltage sinusoidal signal of 30 kHz, whereas the other electrode and the target holder were grounded. We have performed detailed investigation of the voltage and current waveforms, phase differences, volt-current (V-I) characteristics, calculated impedances and power deposition. The aim was to determine the influence of different target materials and their conductivity on the plasma properties. We calculated the total harmonic distortion (THD) factor that showed that the current through grounded electrode depends on the conductivity of the target. We also calculated the power delivered to the plasma core and the plasma plume regions and observed that the change in the target conductance influenced the power in both plasma regions. The experimentally characterized electrical circuit was simulated by a model of equivalent electrical circuit corresponding to the plasma-off and plasma-on regime. Voltage controlled current source was added as model of a streamer formed in plasma-on regime.

Keywords: atmospheric pressure plasma jet, electrical measurements, conductive target, dielectric target, equivalent electrical circuit

1. Introduction

Cold (non-thermal) plasmas at the atmospheric pressure have been proven to be very prospective and useful in a variety of different applications. In some cases, applications of these plasmas are as successful as of plasmas at low pressures [1-3]. The key feature of non-thermal plasmas at atmospheric pressure is the ability to provide a chemically reactive environment in a room-temperature gas and this has facilitated development of numerous plasma applications in biomedicine [4-7]. In this area of applications, one of the most used sources of non-thermal atmospheric-pressure plasma is the plasma jet [8, 9]. Generally speaking, a plasma jet is a technically simple device comprising of a dielectric tube that directs the buffer gas to flow through a limited volume of space where a high electric field is applied. The volume with the high electrical field is usually formed by bringing a high-voltage signal to a conductive wire inserted into the tube or to a conductive surface attached to the outer side of the tube - to serve as a powered electrode. Since in the latter case the electrodes are separated from the plasma region by a dielectric this type of source is called a dielectric barrier discharge (DBD) jet. The other electrode of the jet may be positioned somewhere at the tube or in the vicinity of the tube ending and may serve as a substrate holder. The core plasma is formed inside the tube and as plasma plume exits the tube, it mixes with the air, providing a flux of neutral species (reactive and others), ions, metastables and UV photons. The active species are sustained by the streamer leaving the glass tube and extending deep into the outer region. Outside the tube, from the mixing of the plasma with the surrounding air, different reactive oxygen and nitrogen species (RONS) [10-12] are produced. Plasma sources are particularly advantageous for a number of biomedical and biotechnology applications as they produce small amounts of active species sufficient to induce chains of biochemical events but insufficient to change the entire environment into toxic.

In all applications, plasma jet is positioned in front of the target that is exposed to the flux of reactive particles generated by the plasma [13]. The insertion of a target into the plasma plume region affects the gas flow and, consequently, affects the mixing of the working gas with the air [14]. This, in turn, changes the properties of the plasma and in most situations significantly modifies the delivery of the reactive species to the target.

In cases where a DBD jet has only the powered electrode, target surface connected to the ground also serves as the grounded electrode. The target, then, obviously represents a part of the electrical circuit, thus influencing the plasma. For plasma jets with the grounded electrode positioned at the tube, the plasma is created between two electrodes in the noble gas [15]. Therefore, location of electrodes producing the active plasma is far from the target. However, if the plasma region comes close to or in contact with the target surface, it will start behaving as an additional electrode, changing the electrical circuit, and thereby altering plasma properties similar to a jet with a single (powered) electrode and a grounded target.

As a result, the second important parameter affecting the properties of the plasma produced by jets is the target conductivity [16-18]. It was experimentally shown by observing the optical emission spectra that the target conductivity impacts the densities of excited species in plasma [19-23]. Computational research of the influence of the target conductivity demonstrated that the variation of the conductivity influences electron temperature and

densities of charged and neutral species in the plasma effluent [24]. In addition, the dependence of the impact force of an atmospheric-pressure non-equilibrium plasma jet on different target types has been recently measured [25].

Clearly, target conductivity presents a crucial parameter when it comes to applications. Hence, measurements related to treatments have been conducted, using appropriate targets or their models treated by specific plasma jet configurations [26-28]. In that way, valuable data related to applications have been acquired. However, in most situations, authors studied pin/needle electrode jets or DBD jets with pulsed power. The configuration of a DBD jet with one continuously powered and one grounded electrode is a frequently encountered configuration used in many biomedical applications, as well in the treatment of liquids [29]. Thus, we believe that investigation of the influence of the target conductivity on plasma parameters in this jet configuration is of interest.

Power dissipation is one of the key properties when it comes to the treatment of biological samples and water, as it is connected to the stability and reproducibility of the plasma treatment and the heat transfer to the target [16]. The significance of the power as one of the most important parameters is visible especially in the fields of plasma medicine and plasma agriculture where the comparison of different plasma sources and their efficacy is important. This fact has been recognized by several groups of authors [30-33], so the procedure to establish power given to the plasma requires further research and development of appropriate protocols. The power dissipation in plasma is encountered as one of the open issues in plasma diagnostics. As a rule, the actual power dissipated in the plasma is often quite different from the input power. Especially, the case of DBD plasma jets with two electrodes is intricate since the power dissipated in the effluent that interacts with the target surface is different than the power in the plasma core. Introducing the target produces a power outflux from the plasma [34, 35], whose accurate determination can be a challenging task since suitable signal waveforms cannot be monitored easily.

The principal aim of this work is to investigate the effect of the conductivity and the type of the target surface on the properties of a continuously powered DBD type atmospheric-pressure plasma jet that is operated in front of three different targets: a copper plate, a PET plate and a distilled-water surface. The measurements presented in this paper clarify the link between the conductivity of the targets and the electrical characteristics, namely the voltage-current (V-I) characteristics and power. For all three types of targets, we conducted comprehensive measurements of the average power dissipated between the powered and the grounded electrode, as well as measurements of the average power delivered from the plasma to the grounded target, aiming at determining the power portion directed towards the target. Also, a Simulink MATLAB model was developed to describe an equivalent electrical circuit of the DBD jet. With this model we have given an insight of the electrical circuits (and components) that are describing plasma-off and plasma-on regime, with consideration of three different targets. We present the results of voltage and current waveforms and V-I characteristics obtained for different targets and gas flows. Additionally, power dissipation is discussed with respect to the target type.

2. Experimental setup

The studies presented here have been conducted with a two-electrode DBD jet with He as the working gas. The schematic of the experiment is shown in Figure 1(a). The jet consists of a 20 cm long glass tube, with 6 mm outer and 4 mm inner diameters. To produce a high-voltage signal, a 30 kHz sine signal is sent from a signal generator (PeakTech 4025) to a 'home-built' amplifier and then to a transformer. This high-voltage signal is then supplied to the powered electrode made of a copper (Cu) foil tightly wrapped and glued around the glass tube. The width of the powered electrode is 15 mm and it is positioned 15 mm from the end of the glass tube. The grounded electrode made of the Cu foil is wrapped around the tube 15 mm away from the powered electrode. The flows of 2 slm or 3 slm of Helium are introduced into the tube through a flow controller. In all experiments the jet is positioned vertically, and the target surfaces are placed below the jet tube ending at the distance of d=10 mm (see Figure 1(a)). We have used a Cu plate (thickness 1 mm), polyethylene terephthalate (PET) plates (thickness 2 mm) and 22 ml of distilled water (dH_2O) in a glass Petry dish (Ø 5.5 cm) as target surfaces. In the case of the PET target, we have used 3 plates in a stack (total thickness of 6 mm).

For all measurements presented here the plasma plume is touching the target surface (see Figure 1(b)). Plasma was in a glow regime if looked at by a naked eye for all plasma operating conditions. In case of all three targets with the voltage increase one conductive channel is formed along the tube axis with its emission intensity increasing with the voltage. Even for maximum applied voltages and for Cu target we did not see the formation of separate filaments. Nevertheless, the time resolved ICCD images show for this type of APPJ that depending on the conditions like water vapor percentage, percentage of surrounding air mixing with helium, applied power, we can detect formation and propagation of Pulsed Atmospheric-pressure Plasma Streamers (PAPS) [15, 36].

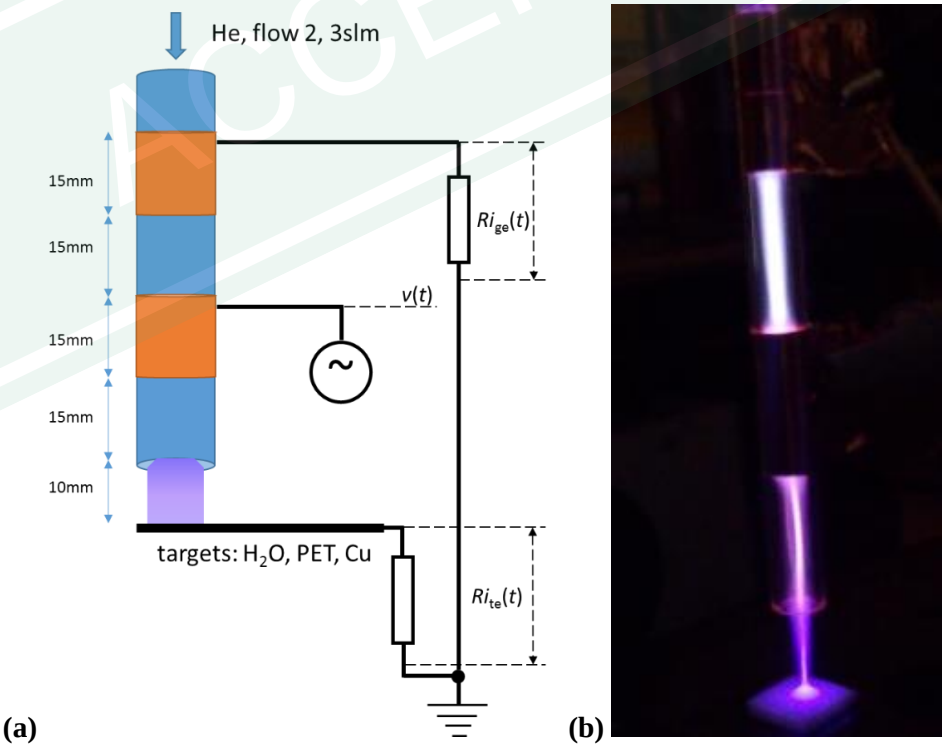

Figure 1. (a) Schematics of the experimental setup. Dashed lines present the measurement points of the supplied voltage *v(t)*. Voltages on R=100 kΩ resistors are used for monitoring the grounded electrode current $i_{ge}(t)$ and the target current $i_{te}(t)$. (b) Image of He plasma jet operating.

All three targets were grounded through a resistor (R=100 kΩ). The electrical conductivity and relative permittivity for the targets are given in Table 1 [37-40]. The general relation between the permittivity and conductivity is the following:

$$\varepsilon(\omega) = \varepsilon'(\omega) + j\varepsilon''(\omega) = \varepsilon_r(\omega)\varepsilon_0 + j\frac{\sigma(\omega)}{\omega}, \quad (1)$$

where $\varepsilon_r(\omega)$ is relative permittivity, ε_0 is vacuum permittivity, ω is frequency and $\sigma(\omega)$ is the conductivity. As seen from Table 1, in case of Cu target, the conductivity is the one responsible for the system behaviour while in the case of PET it is the permittivity. As it should be expected, in the case of water both parameters are almost equally influencing the system behaviour.

Table 1. Electrical conductivity and relative permittivity of the targets

Target	Electrical conductivity, σ [S/m]	Relative permittivity, ε_r	ε'	ε"	Dominant term in eq. (1)
Cu plate [37]	$6\cdot10^{7}$ (1)	1	~10^{-12}	~j10^{2}	Im part i.e., conductivity
Distilled H_2O [38]	$5\cdot10^{-6}$ (2)	80 (3)	~10^{-10}	~j10^{-11}	Both Re and Im
PET plate [39, 40]	10^{-21} (1)	3–4.5 (4)	~10^{-11}	~j10^{-26}	Re part i.e., permittivity

The Cu plate exposed to the ambient air was unprocessed and unpolished before it was used as a target, so one may presume that an oxide layer, whose conductivity is relatively low (in the range of that for semiconductors), is formed on the surface.

Nevertheless, we perform treatment of the surfaces by plasma before measurements to remove organic and other complex contaminants, to clean the surface from deposited materials and to make the surface more uniform without hoping that we have removed completely the oxide layer on the surface [41, 42]. After the plasma treatment of the surface the influence of possible variations of the properties of the surface layer on the plate conductivity is negligible. Similarly, clean PET plates are exposed to the preconditioning treatment before each measurement set and no visible change of the plate surface after the measurement has been observed. For dH_2O samples, the water

conductivity was determined before the measurements and it did not change during the short duration of the measurements. We used Hanna Instruments (HI76312) conductivity probe with Hanna Instruments controller HI5521 to monitor the conductivity of the water target. Therefore, the stability of target surfaces is adequate so that it does not affect the plasma during measurements in all cases.

The electrical measurements were done at three points in the electrical circuit (see Figure 1(a)). The voltage signal supplied to the jet $v(t)$ was measured with a high-voltage probe (Tektronix 6015A) attached to the powered electrode of the jet. Both currents, from the grounded electrode $i_{ge}(t)$ and the target $i_{te}(t)$, were monitored by measuring the voltage drops (Agilent 10076C) on the 100 kΩ resistors and are recorded separately. These recordings allowed observing electrical waveforms during plasma operation, to obtain the RMS values of the voltage and currents and, eventually, to calculate the power transmitted to the plasma. All measurements were repeated, and we have obtained stable and reproducible operation of the plasma in the whole range of conditions investigated.

During initial measurements we monitored the humidity in the gas flow by using a dew point meter (Vaisala DMT 143). The abundance of the H_2O vapor proves to be an important parameter that influences the plasma conditions [43, 44]. We observed that after 10-15 minutes of operation, the humidity dropped to ~15 ppm and stayed at that value throughout the experiment. Thus, we adopted a procedure for preconditioning the jet before each measurement set that includes 10 minutes of plasma operation with an appropriate target at a moderate value of the applied voltage.

ACCEPTED

3. Results and discussion

3.1 Equivalent electrical circuit

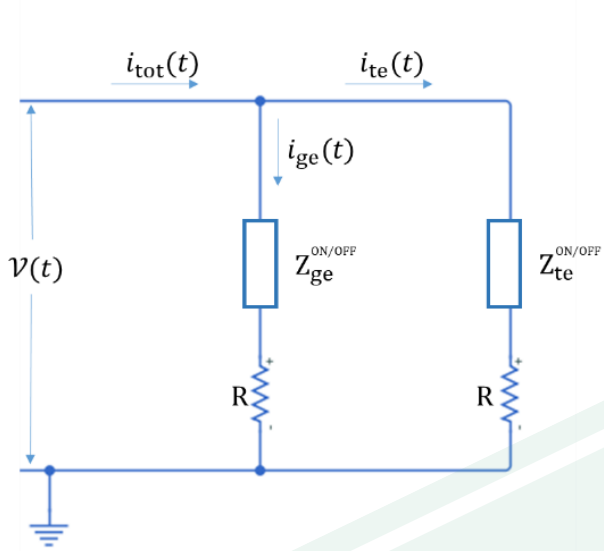

Figure 2. Experimental equivalent electrical circuit of DBD plasma jet.

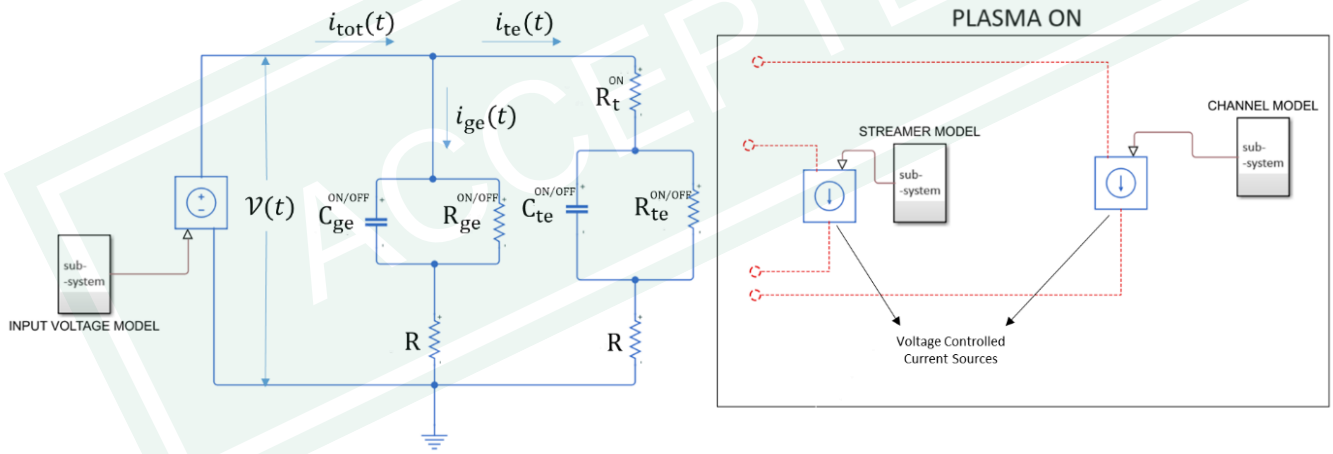

Figure 3. Detailed model of the equivalent electrical circuit made in MATLAB Simulink. When plasma is ignited, additional voltage controlled current sources must be added due to the occurrence of PAPS (streamer). Then the additional elements to the circuit are shown on the right-hand side in the schematics denoted with PLASMA ON.

In general, the electrical circuit of the DBD plasma jet can be represented as shown in Figure 2. Impedance Z_{ge} represents total impedance in the first branch (plasma core) of electrical circuit consisting of two electrodes wrapped around the glass tube. Z_{te} represents total impedance in the second branch (plasma plume) of electrical circuit with

the target. Both Z_{ge} and Z_{te} can be calculated from the V-I characteristics. The ON and OFF annotations represent plasma on (discharge working in stable mode) and plasma off (no discharge) cases.

To better understand the behaviour of the plasma system we have developed a more detailed model of equivalent electrical circuit by using Matlab Simulink. The schematics of the circuit is shown in Figure 3. All elements are denoted in similar manner as the impedances in Figure 2. The first branch represents electrical properties of the powered and grounded electrode wrapped around the glass tube (capacitance C_{ge} and resistance R_{ge} in parallel) and second represents the target (capacitance C_{te} and resistance R_{te} in parallel).

Electrical components of the equivalent circuit and their values are presented in Table 2. The values obtained from the equivalent electrical circuit model give the current and voltage waveforms that are in 99% agreement with the measured ones. When applied voltage *v(t)* is below the breakdown threshold for plasma ignition (Plasma-OFF), equivalent electrical circuit of the DBD jet is shown in the left-hand side of the Figure 3. In Plasma-OFF regime, if we change the target, thus changing the electrical properties, the electrical circuit representing the core of plasma does not change (C_{ge}, R_{ge}). This is an expected behaviour because a two-electrode DBD jet is basically a simple capacitor filled with gas. The capacitance C_{ge} represents the capacitance due to the dielectric material of the tube (C_{wall}) and also due to the volume of the discharge tube (C_{gas}). The change of target material influences only part of the electrical circuit that includes the target where we can see small changes in C_{te} and R_{te}.

Table 2. Parameters of equivalent electrical circuit

		R [MΩ]	R_{ge} [MΩ]	C_{ge}[pF]	R_t[MΩ]	R_{te}[MΩ]	C_{te}[pF]
Plasma OFF	*Cu*	0.10	6.80	1.50	/	10	1.00
	dH_2O	0.10	6.80	1.50	/	13	0.75
	PET	0.10	6.80	1.50	/	11	0.85
Plasma ON	*Cu*	0.10	2.20	1.50	2.80	7	1.50
	dH_2O	0.10	2.10	1.70	3.50	7	1.25
	PET	0.10	2.20	1.35	3.50	/	1.40

Plasma ignition (Plasma-ON) introduces significant changes to the circuit in both branches. The capacitances of both branches (plasma core and plasma plume) are changed depending on the electrical characteristics of the targets and formation of the plasma sheaths. At the same time the resistances (R_{ge}, R_{te}) are decreased due to the breakdown

and plasma ignition. When target is PET, the almost ideal insulator, target is represented only as capacitor C_{te} (R_{te} is zero). In plasma plume branch after plasma ignition, we have a new element R_t representing mainly the energy dissipation in plasma plume and trough the target. The appearance of PAPS is modelled by the voltage controlled current source [45-47] shown in right-hand side of Figure 3 (streamer model). The PAPS appear only in the positive half-period of the voltage signal [15, 36]. In similar DBD jet configuration, in negative half-period of the voltage signal we did not observe PAPS, but a formation of a continuous plasma channel that starts at the target and spreads towards powered electrode of DBD jet [48]. This plasma channel is modelled by the second voltage controlled current source Figure 3 (channel model).

3.2 Electrical measurements

We have performed full electrical characterization of the DBD jet with a grounded target surface positioned underneath. Three different signals were monitored in time: the voltage supplied to the powered electrode $v(t)$, the current flowing between powered and grounded electrode $i_{ge}(t)$ and the current passing through the plasma plume into the target $i_{te}(t)$. As the current $i_{ge}(t)$ effectively describes the region between the electrodes, we may attribute these values to the plasma core, while the other current, $i_{te}(t)$, provides an insight into the plasma plume, the region of the plasma between the core and the target.

In Figure 4 we show waveforms obtained at 2 slm of He and three different targets. These waveforms were obtained for each target when the discharge is ignited by the same voltage as indicated at the signal generator. The left-hand side y-axis shows values of $v(t)$, while the right-hand side shows values of $i_{ge}(t)$ and $i_{te}(t)$. Vertical dashed lines in the plots mark the time-point of one maximum of $v(t)$ signal to assist the observation of the time-shift between the voltage and current signals. The period of the $v(t)$ signal is T=33 μs.

ACCEPTED

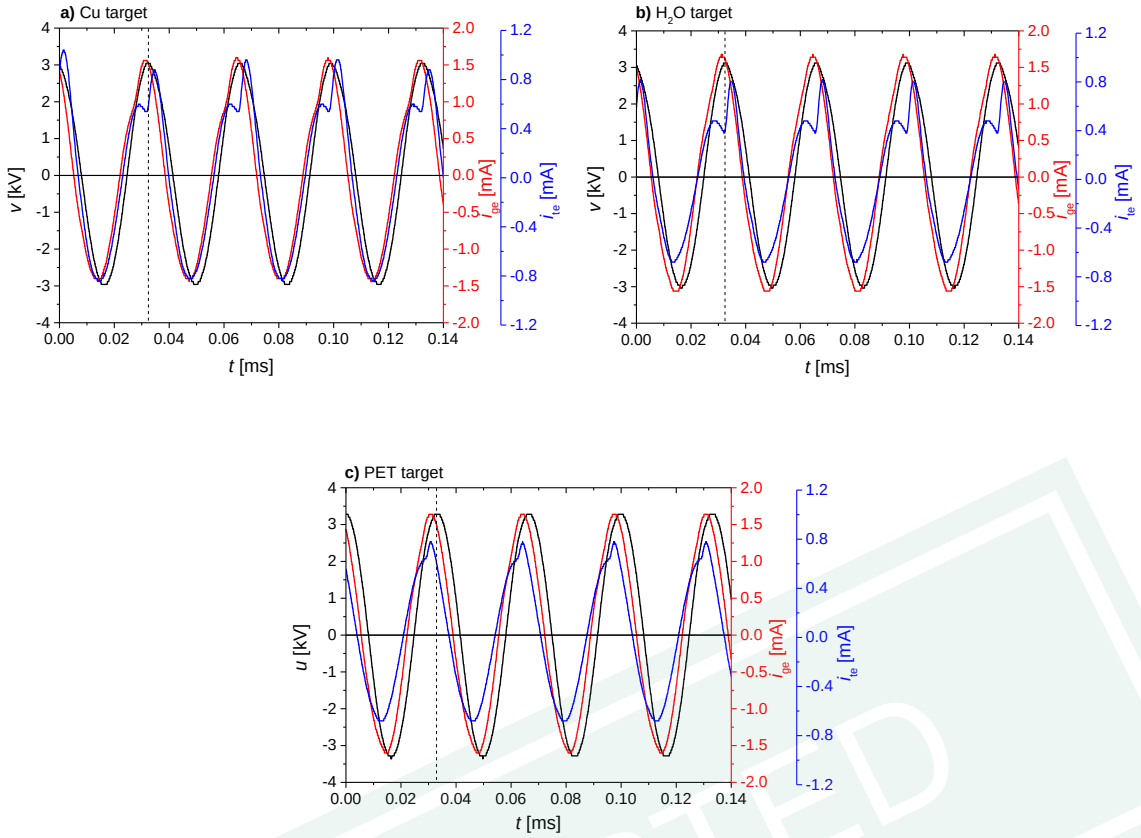

Figure 4. Waveforms of voltage *v(t)* (left-hand side), grounded electrode current $i_{ge}(t)$ and target electrode current $i_{te}(t)$ (right-hand side) recorded for three different targets and flow of 2 slm of He. Vertical dashed lines mark the time-point of one maximum of the *v(t)* signal.

For all three targets the current signals ($i_{ge}(t)$, $i_{te}(t)$) precede the voltage signal indicating that this is a predominantly capacitive system. This is even more pronounced when the plasma is not ignited. In that case both currents, that pass through the grounded wrapped electrode and through the target, precede the voltage waveform and they are influenced mainly by the geometry of the electrodes and position of the target. The phase differences in the plasma-off case are ~55° for the grounded electrode and ~50º for the target electrode. These values differ from the 90º phase difference that is expected for a purely capacitive impedance, due to resistance of the components of the electrical circuit and the plasma jet.

When the discharge is ignited, the current $i_{ge}(t)$ through the grounded electrode precedes the voltage signal for $\Delta\tau$=2.55 μs, which corresponds to the phase shift of ~28º. This phase shift is not influenced by the type of target indicating that the parameters of the plasma core inside the tube are mainly governed by the inter-electrode distance and geometry. On the other hand, the current passing through the target is highly influenced by the type of the target and its characteristics, as expected. The phase differences between $i_{te}(t)$ and *v(t)* are ~14º, ~28º and ~41º for the Cu, dH_2O and PET target, respectively. The increase in the phase shift corresponds to the decrease in the conductivity of the target.

3.2.1 V-I characteristics

To get a clearer picture of the nonlinearity that plasma introduces into the system, we have analysed the signals in the frequency domain by using the Fast Fourier transform. When plasma is not ignited, all three signals for all three targets have only the fundamental harmonic (1st harmonic), as expected. When plasma is ignited, the nonlinearity introduced into the system by the plasma can be evaluated through the total harmonic distortion factor (THD). THD is calculated as

$$THD = \frac{\sqrt{\sum_{n=2}^{\infty} V_{n_{RMS}}^2}}{V_{fund_{RMS}}} \cdot 100(\%) \qquad (2)$$

where V_{n_RMS} are root mean square (RMS) values of the higher harmonics (n=2, 3…) and V_{fund_RMS} is the RMS value of the fundamental harmonic at f=30 kHz. The same formula was used for I_{ge} and I_{te}.

Table 3. THD percentages for voltage and current signals

Target	*THD_V* (%)	*THD_I*ge (%)	*THD_I*te (%)
Cu	0	18.2	38.2
dH_2O	0	13.4	46
PET	0	7.3	13.5

The calculated THD values are shown in Table 3. While the voltage waveform is not distorted, the THD percentage for the current going through the grounded electrode (I_{ge}) depends on the conductivity of the target. In Table 3 we can see that the highest distortion (THD_I_{ge}) in the signal is obtained for the Cu target and generally it increases when target's conductivity increases. The situation with I_{te} is somewhat different, as it is in correlation with the effective conductivity, which also depends on the stability of the material of the target surface and/or fluctuations in plasma-surface interactions. The highest THD was obtained for the dH_2O target. This indicates that during the plasma operation the target surface is changing significantly due to the helium gas flow, evaporation, and the plasma-water interface interactions. The high instability of the dH_2O surface results in the appearance of a large number of significant harmonics (up to n=14) present in the signal. On the other hand, for the Cu target there are n=6 significant harmonics and for PET only n=3 (n includes the 1st harmonic). The appearance of the higher harmonics can also be anticipated since there is a visible variation in the I_{te} signal shape at positive peak value.

To facilitate the comparison of time-varying signals, the RMS values of waveforms should be calculated. In case of the voltage, the RMS values were calculated using:

$$V_{RMS} = \sqrt{\frac{1}{nT}\int_0^{nT} v^2(t)dt} \qquad (3)$$

Calculation of the RMS values for the currents was conducted in a similar manner. In all calculations, seven periods were used (n=7).

In Figure 5 we show V-I characteristics of the DBD jet measured for three targets and 2 slm of the He flow. Figures 5(a–c) show the dependence of the voltage on the current flowing through the grounded electrode (I_{ge}), and Figures 5(d–f) present the V-I characteristics depending on the current through the target (I_{te}). The measurements are performed starting with voltages lower than the breakdown voltage and then increasing gradually to the maximum voltage of the power supply (shown in solid symbols). Then, from the maximum voltage of the power supply it is decreased to the starting voltage (shown with open symbols). The increment and decrement of the applied voltage is accomplished in steps, sweeping over the same values.

The V-I characteristics for low voltages, when the plasma is not ignited, are linear since the impedance depends only on the characteristics of the electrode system, mainly on its capacitance. In all V-I characteristics there is a drop of the V_{RMS} values at the point where plasma is ignited. As expected, the current flowing through the grounded electrode is higher than the current through the target. After ignition, the main plasma core is constrained inside the jet, between the electrodes wrapped around the jet tube. Here, the gas mixture consists of helium with only a small amount of air impurities in which the breakdown occurs. Then plasma spreads towards the end of the tube where the percentage of air in the mixture is higher. Having crossed some distance in the external region, the plasma gets in contact with the grounded target surface.

From Figures 5(a–c) we can see that the impedance is not constant for the whole range of the applied voltages due to the changes introduced by plasma. The nonlinearity of the impedance is more evident in the V-I curves for the grounded target (Figures 5(d–f)), especially for the Cu and dH_2O targets. For lower applied voltages and currents the plasma plume is a glow type. With an increase in the applied voltage an apparent conductive channel is formed whose emission intensity increases with the voltage. After the channel formation, the applied voltage increases slower than the current through the plasma plume. This is represented in the V-I curves as a change of the impedance to a lower value. The plasma behavior and V-I points do not change in measurements when the input voltage is decreased (Figures 5(a–f), open symbols). The only difference with respect to the increasing-voltage case is that the plasma stays ignited till lower voltages are reached, thus producing a hysteresis effect. The hysteresis as shown in Figure 5 is often observed for plasma discharges. What is interesting here is that the hysteresis depends strongly on the material of the target and seems to be the largest for water target.

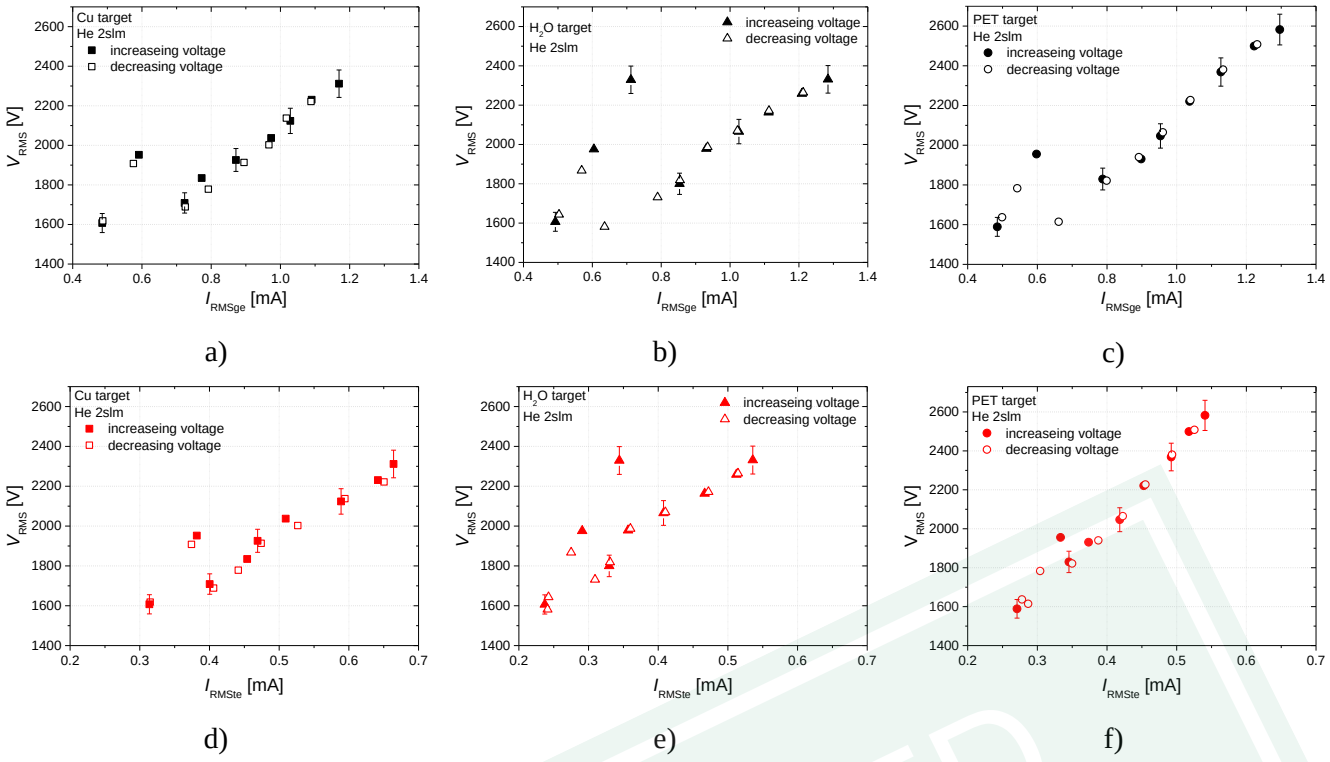

Figure 5. V-I characteristics of the He DBD jet plasma in contact with 3 different targets. Solid symbols are points obtained by increasing the input voltage, while open symbols are obtained by decreasing the voltage. Plots (a) – (c) present the dependence of the RMS voltage on the current through the grounded electrode I_{RMSge} and (d) – (e) the dependence on the current through the target I_{RMSte}.

For a better comparison, the V-I characteristics obtained for the different targets are presented together in Figure 6. The voltage dependance on the current through the grounded electrode are given in Figure 6(a) and the dependance on the current through the target in Figure 6(b). The points acquired after the plasma ignition are marked by open symbols and connected with a line to make the data more legible.

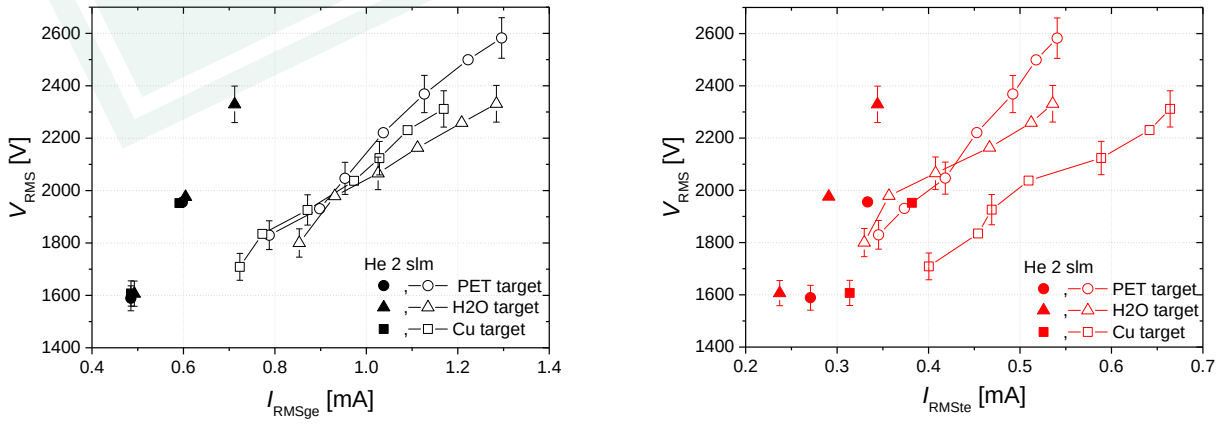

Figure 6. V-I characteristics of the DBD jet in contact with 3 different targets. The dependence of V_{RMS} is plotted against (a) grounded electrode current, (b) target current. The open symbols are measured with the plasma ignited and they are connected by lines to improve legibility.

The data points obtained without plasma for the targets fall on top of each other, as shown in Figure 6(a). Obviously, before the breakdown, the impedance is the same for all three targets (Z_{ge}=3.3 MΩ) and this is also confirmed by components (C_{ge}, R_{ge}) obtained by Simulink model. As observed in the previous section, after the plasma ignition, the voltage drops significantly for all the targets and regimes of operation, i.e., the voltage and current obviously depend on the type of the target. For the Cu target, the plasma after ignition initially operates at around 1700 V, while the current flowing between electrodes is around 700 μA. This is the lowest plasma operation voltage and current for all three targets. The reason lies in the high conductivity of the target that enables efficient breakdown and discharge operation. For the case of the PET target, the voltage after ignition is around 1830 V and the current is at 800 μA (see Figure 6(a)). A similar operating voltage of around 1800 V is also obtained with the dH_2O target, while the current immediately goes to around 850 μA.

Slopes of the V-I characteristics of the core plasma after plasma ignition change in a different manner, depending on the target (Figure 6(a)). The curves obtained for the PET and dH_2O targets both change the slope in the 0.9 mA–1 mA interval, while for the Cu target the change is observed around 0.8 mA. By assessing the recorded waveforms that are used to obtain points of the V-I characteristics we could observe only variation in the amplitude of the waveforms. The slope change (i.e., the impedance change) is due to the nonlinear changes of charge densities in the plasma that may originate from different reaction kinetics in the gas phase and/or effects of the surface charges [49, 50]. We could not observe any additional distortion of the waveforms that has been detected by other authors in the case of the plasma mode transition [51-53].

The points of the plasma plume V-I characteristics obtained before plasma ignition differ significantly with the targets used (Figure 6(b)). After ignition, the highest RMS current values (I_{te}) are recorded for the Cu target. This can be explained by a considerable amount of charged particles that are efficiently transferred to the plasma plume. In the case of PET and dH_2O targets the maximal measured currents are similar. However, the RMS voltages depend on the target's conductivity. For the PET target the impedance is constant for all applied voltages. However, for the dH_2O and Cu targets the impedances change and this corresponds to an appearance of a stronger, more intense, conductive plasma channel.

In Figure 7 we show the V-I characteristics obtained for the PET and dH_2O targets at two different He flow rates: 2 slm and 3 slm. Points obtained with ignited plasma are connected by lines. The variations in He gas flow affect the V-I characteristics for these two targets, but they do not introduce significant changes for the Cu target. With the Cu target the plasma plume impinges on a highly conductive surface, which may result in the occurrence of a stronger gas flow of He between the jet tube and the target [54, 14]. Thus, relatively small changes in the gas flow rate (between 2 slm and 3 slm) cannot modify the electrical properties of the jet.

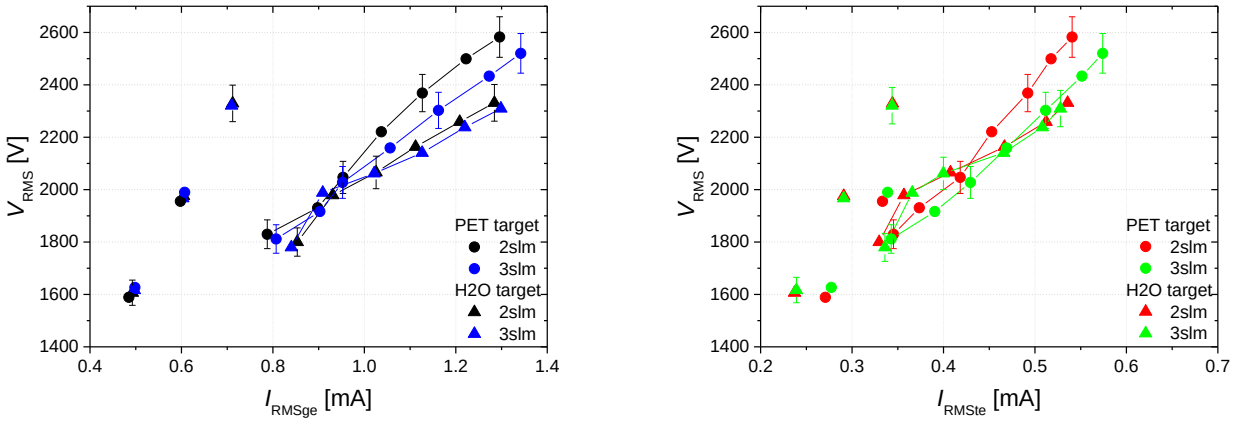

a) b)

Figure 7. V-I characteristics of the DBD jet in contact with PET and dH2O targets at two He flow rates. The dependence of V_{RMS} is plotted against (a) grounded electrode current, (b) target current. Lines connect the points obtained when plasma is ignited to improve legibility.

For the V-I characteristics of the plasma core part, i.e., for the voltage dependence on the current through the grounded electrode, in the case of the water target there is a very small difference between the operating points obtained at different flow rates (Figure 7(a)). For the currents below 1.1 mA the curves are indistinguishable, while at higher currents the difference is of the order of the voltage measurement error (around 20 V). However, for the PET target there are bigger differences in the operating voltages at different flow rates. For jet currents above 0.9 mA, voltages may be different as much as 100 V. The V-I characteristic of the plume region, i.e., the voltage dependence on the current through the target, shown in Figure 7(b), has a similar dependence as in Figure 7(a). In the plume region the V-I characteristics in the case of dH_2O do not change with the gas flow, while for the PET target the operating voltages become different for the currents above 4 mA. Hence, the pronounced difference in the V-I characteristics of both regions measured at different flow rates is observed only for the PET target. Since the effect of the surface charges is pronounced on the PET target, these results indicate that the surface charges can affect both the plasma plume region and the plasma core. This has been thoroughly studied in the case of the pulse-powered jets [24, 26, 55]. In papers [18, 56] it has been shown that for low-permittivity dielectric targets (such as PET) there is a rapid charging of the surface and formation of surface ionization waves. Additionally, properties of the dielectric target influence not only the density of electrons, i.e., the electric field, but also the density of radicals in the plume region [57]. In our case of continuous power supply, the same processes occur, but may be diminished due to short plasma-off time in comparison to the low-duty cycle pulsed discharges. Nevertheless, a strong influence of the low-permittivity PET target on both the electron and neutral species in the plasma plume is reflected in the plasma core, resulting in visible differences in the V-I characteristics obtained with the two He flow rates. For the case of a pulse-powered jet in contact with high-permittivity dielectric (H_2O target), authors discuss the existence of a return stroke (or 'third' discharge) due to the high electron production and enhancement of the electric field adjacent to the substrate surface [18, 57]. On the other hand, in the situation with continuously powered jet against

a grounded conductive target, the appearance of anode directed streamers has been observed but only in a narrow range of operating conditions [48].

3.2.2 Power transmitted to the discharge

Another important parameter that describes interactions between the plasma and the target is the power delivered to the discharge and then forwarded to the target. In this study, as the first step in power assessment, time-dependent power signals are obtained. The instantaneous power is calculated from the voltage and current waveforms (as shown in Figure 4). Since we recorded both the current between powered and grounded electrode $i_{ge}(t)$ and the current passing through the plasma plume into the target $i_{te}(t)$, powers delivered to the core of the plasma and from the plume to the target could be calculated. The following formula is used for calculation:

$$p(t) = v(t) \cdot i_k(t) \tag{4}$$

providing the appropriate current waveform is used (denoted by index *k*).

The instantaneous power calculated using plasma-on waveforms also contains the power losses in the plasma jet circuitry [58]. To separate this part, several approaches could be used. For instance, at a specific current, the input power without plasma could be measured allowing an estimate of the power losses [58, 59]. Another approach applied here is to subtract the effect of the displacement current, assuming only stray capacitance of the plasma source from calculated circuit impedance [60]. Then, the time-averaged power is obtained from the equation:

$$P_k = \frac{1}{nT}\int_0^{nT} p(t)dt \tag{5}$$

The calculated powers are plotted against the RMS voltages for the Cu, dH_2O and PET targets at 2 slm of He in Figure 8. P_{ge} shown in Figure 8(a) is the average power dissipated between powered and grounded electrode (in the plasma core region), while in Figure 8(b) we calculated P_{te} as the average power delivered from the plasma to the grounded target (plasma plume region). The lowest plasma core power of 1.1 W is obtained for the Cu target at the lowest operating voltage of 1700 V. The highest power is for the PET target, i.e 3 W at 2580 V RMS (Figure 8(a)). The powers calculated for all three targets in the RMS voltage range from 1900 V to 2100 V are very similar. For higher voltages, the discrepancy is more pronounced. The highest power dissipated at a specific voltage is for the water target and the lowest power is for the PET target. These results are in accordance with the V-I characteristic (Figure 6(a)). In the plume region, the lowest power of 0.5 W is measured for the PET target and the highest power of 1.5 W is obtained for the Cu target (Figure 8(b)). Unlike the power dissipated in the plasma core (Figure 8(a)), here the lowest and the highest powers are not correlated with the extreme values of operating voltages. These results agree well with the V-I characteristic in Figure 6(b) − at a particular operating voltage, the highest current is achieved for the Cu target and hence the highest powers in Figure 8(b) are also obtained for this target. The power from the plasma plume dissipated to the target (P_{te}) strongly depends on the target type, with a difference between the minimal and maximal power of more than 40 % at around 2300 V. For voltages below 2100 V powers measured

for a high-permittivity dielectric (dH_2O) and a low-permittivity dielectric (PET) are almost the same. Concerning the dependence of P_{ge} and P_{te} on the respected currents, as slopes of the V-I characteristics obtained for all 3 targets showed similar rising tendency (Fig.6), the dependence of power Pge on grounded electrode current and power Pte on target current would be similar to the dependences on voltages plotted in Fig. 8 with slightly different slopes. Calculated P_{ge} values would correspond to the RMS values of grounded electrode current from 0.7 mA to 1.3 mA while for P_{te} values the target current range would be from 0.35 mA to 0.65 mA.

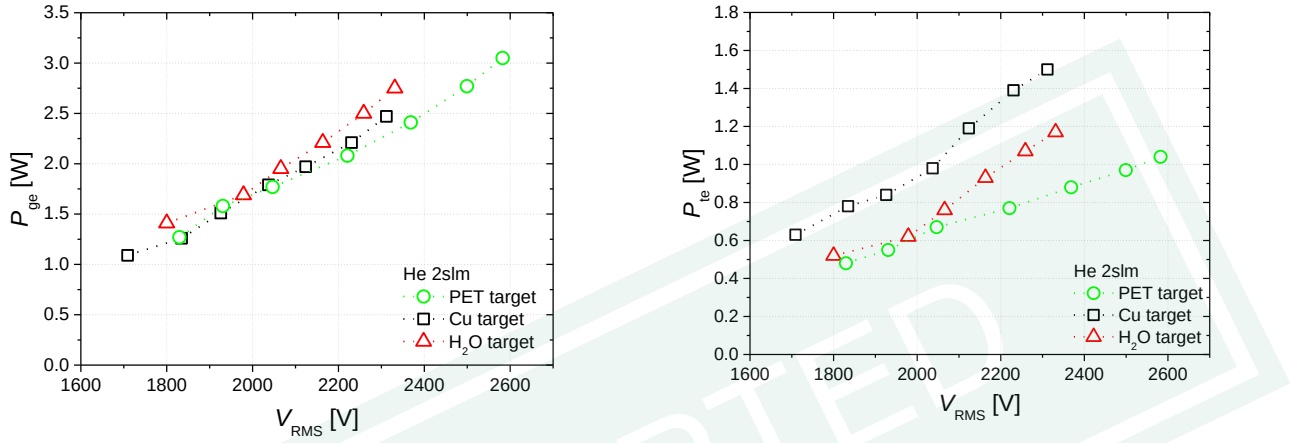

a) b)

Figure 8. The average power as a function of the RMS voltage in the case of Cu, dH_2O and PET targets at 2 slm of He. a) Average power dissipated between the powered and grounded electrode (plasma core region) and b) average power dissipated from the plume to the grounded target (plasma plume region).

To estimate the efficiency of transferring the power from the plasma core to the plasma effluent in contact with the target, we calculated the ratio of the average power dissipated between the powered and the grounded electrodes to the average power delivered from the plume to the grounded target. This power transfer efficiency as a function of the RMS voltage is shown in Figure 9. The obtained values clearly show the changes in plasma behavior related to the target conductance.

For the copper target, more than 50 % of the plasma core power is delivered to the plume region and the target, while for the dielectric targets (PET and dH_2O) these percentages are around 35 %. The reason for this is twofold. One is the combination of a strong conductive channel impinging upon conductive material results in high power delivered to the target. This is also visible in the V-I measurements plotted with I_{te} (Figure 6(b)) where the current obtained for Cu target is higher than for other two materials. The highest conductivity led to the highest currents. Apart from the current and voltage amplitudes their phase difference will determine the average power delivered to that part of the circuit. In case of Cu target the phase, difference is 2 and 3 times smaller compared to the phase differences in case of dH2O and PET, respectively. Thus, one can assume that there is a threshold conductivity of the target below which the power ratio appears to be the same regardless of the conductivity.

ACCEPTED

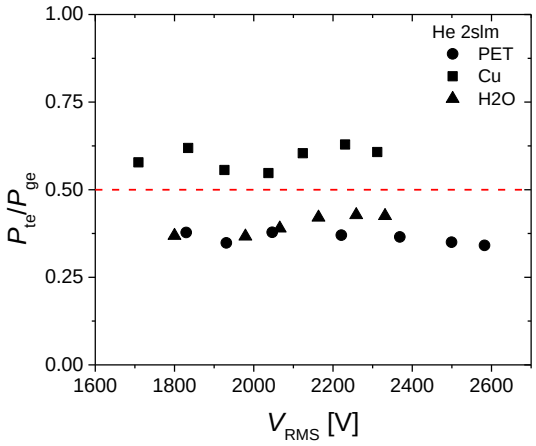

Figure 9. Ratio of the power dissipated in the plume (passing through the target) and the power in the plasma core region for three different targets: PET, Cu and dH_2O. The results are obtained for 2 slm of He.

Values of the power ratio for the Cu target oscillate, i.e., the efficiency curve presented in Figure 9 has inflections. In the case of the water and PET targets, the ratios are nearly the same below 2100 V. Above that voltage, the ratio for dH_2O stays around 40 %, while the values for PET decrease slightly reaching 35 %. This difference between the dielectric targets at higher voltages is also visible in Figure 6(b) and Figure 8(b). Considering the presented results, the efficiency of the power transfer is one of the important parameters that should be considered when performing treatments with conductive or dielectric substrates.

4. Conclusion

In this paper we presented detailed electrical characterization of a DBD plasma jet in contact with three different types of targets: a conductive Cu plate, a PET plate (low electrical-permittivity sample) and distilled H_2O (high-permittivity sample). The analysis included an equivalent electrical circuit model that emphasizes differences between plasma-off and plasma-on regime (by including voltage controlled current source representing a streamer with a leading ionisation and tail back to the electrode). Small changes in electrical elements corresponding to the target's electrical properties (C_{te}, R_{te} and R_t) are also observed.

The experimental setup allowed us to record the high-voltage signal supplied to the jet and two currents. One current was recorded at the grounded electrode $i_{ge}(t)$, while the other was in the line connecting the target and the ground $i_{te}(t)$. In both cases the currents were separately monitored by measuring the voltage on 100 kΩ resistors. In this way we were able to obtain waveforms from the core and plume regions of the plasma. Using the waveforms, plasma-induced nonlinearity in the sine signal was assessed and described using the total harmonic distortion factor (*THD*). The voltage waveform was not distorted, but the *THD* for the grounded electrode current (I_{ge}) was shown to depend on the conductivity of the target. The highest distortion in the I_{ge} signal is obtained for the Cu target and

for other dielectric targets the distortion is increased with the increase of the target conductivity. For the current passing through the target (I_{te}), the situation was somewhat different and *THD* did not appear to be directly in correlation with the target conductivity, but with the target surface stability and/or plasma-surface interactions. Moreover, we assessed the phase shift between the voltage and currents waveforms. Only for I_{te}, the phase shift changed when we exchanged the target type. The observed increase in the phase shift corresponded to the decrease in the conductivity of the target.

Using the recorded time-varying signals, we calculated appropriate RMS values and plotted V-I characteristics for two plasma regions: the plasma core and plasma plume. The V-I characteristics were obtained for two gas flow rates. From plasma-off measurements we were able to calculate the impedance of the plasma source. The changes in slopes of the V-I characteristics occurred due to the nonlinear variations of the charge density at different currents, which, in turn, affected the amplitudes of the waveforms and consequently RMS values. We could not observe any additional distortion in the waveforms that was detected by other authors in the case of plasma mode change. The influence of the He flow rate on the V-I characteristics was clearly visible only for the PET target, while the effect is barely present for the dH_2O target. In the case of the Cu target we could not observe any change in the V-I characteristics for the two flows investigated.

By calculating the instantaneous power, we obtained the average power delivered to the plasma core region P_{ge} and the plume region P_{te}. The values obtained for P_{ge} were similar for different targets, while the P_{te} values had considerable differences depending on the targets. The highest power was delivered to the conductive type of target, i.e., the Cu plate. For dielectric targets the calculated powers were lower from 30 % to 40 % in comparison to the Cu target, showing weak dependence on operating voltage and the target. To estimate the power transfer efficiency between the core plasma and the plasma effluent that was in contact with the target, we calculated the ratio of powers in these two regions. The ratio of the average powers P_{te}/P_{ge} showed that the efficiency of the power transfer was higher for the Cu target and lower for PET and dH_2O targets, with similar ratios for these two dielectric targets.

Acknowledgements

K.K. was financially supported by the Hungarian Scientific Research Fund (Grant NKFIH-K132158). N.P., N. Š and M.P. are financially supported by the Science Fund, Republic of Serbia, 7739780, APPerTAin-BIOM project and by the MSTDI Republic of Serbia grant no. 451-03-47/2023-01/ 200024. Z. Lj. P. is grateful to the SANU project F155 for partial support. We thank Ms. Vera Furtula for performing a part of the electrical measurements.

References

[1] Adamovich I et al 2022 *J. Phys. D: Appl. Phys.* 55(37), 373001

[2] Ostrikov K, Cvelbar U and Murphy A B 2011 *J. Phys. D: Appl. Phys.* 44 174001

[3] Makabe T and Petrovic Z Lj 2016 Plasma Electronics: Applications in Microelectronic Device Fabrication (2nd Edition CRC Press)

[4] Stoffels E, Flikweert A J, Stoffels W W and Kroesen G M W 2002 *Plasma Sources Sci. Technol.* 11 383–8

[5] Graves D B 2017 IEEE Trans. Rad. Plasma Med. Sci. 1(4) 281-292

[6] von Woedtke T, Laroussi M and Gherardi M 2022 *Plasma Sources Sci. Technol.* 31 054002

[7] Miletić M, Mojsilović S, Okić Đorđević I, Maletić D, Puač N, Lazović S, Malović G, Milenković P, Petrović Z Lj and Bugarski D 2013 *J. Phys. D: Appl. Phys.* 46 345401

[8] Choi E H, Hong Y J, and Kaushik N K 2021 30(5) 118-136

[9] Winter J, Brandenburg R and Weltmann K-D 2015 *Plasma Sources Sci. Technol.* 24 064001

[10] Stancampiano A, Selaković N, Gherardi M, Puač N, Petrović Z Lj and Colombo V 2018 *J. Phys. D: Appl. Phys.* 51 484004

[11] Gerber I C, Mihaila I, Hein D, Nastuta A V, Jijie R, Pohoata V and Topala I 2017 *Appl. Sci.* 7 812

[12] Oh J-S, Aranda-Gonzalvo Y and Bradley J W 2011 *J. Phys. D: Appl. Phys.* 44 365202

[13] Lu X, Naidis G V, Laroussi M, Reuter S, Graves D and Ostrikov K 2016 *Phys. Rep.* 630 1–84

[14] Robert E, Sarron V, Darny T, Riès D, Dozias S, Fontane J, Joly L and Pouvesle J-M 2014 *Plasma Sources Sci. Technol.* 23 012003

[15] Maletić D, Puač N, Malović G, Đorđević A and Petrović Z Lj 2017 *J. Phys. D: Appl. Phys.* 50 145202

[16] Hofmann S, Van Gils K, van Der Linden S, Iseni S and Bruggeman P 2014 *Eur. Phys. J. D* 68 56

[17] do Nascimento F, Moshkalev S and Machida M 2017 *Braz. J. Phys.* 47 278–287

[18] Klarenaar B L M, Guaitella O, Engeln R and Sobota A 2018 *Plasma Sources Sci. Technol.* 27 085004

[19] Zaplotnik R, Bišćan M, Kregar Z, Cvelbar U, Mozetič M and Milošević S 2015 *Spectrochimica Acta Part B* 103-104 124-130

[20] Kovačević V V, Sretenović G B, Slikboer E, Guaitella O, Sobota A and Kuraica M M 2018 *J. Phys. D: Appl. Phys.* 51 065202

[21] Yamada H, Sakakita H, Kato S, Kim J, Kiyama S, Fujiwara M, Itagaki H, Okazaki T, Ikehara S, Nakanishi H, Shimizu N and Ikehara Y 2016 *J. Phys. D: Appl. Phys.* 49 394001,

[22] Nastuta A V, Pohoata V and Topala I 2013 *J. Appl. Phys.* 113(18) 183302

[23] Shershunova E A, Moshkunov S I and Khomich V Y 2019 *IEEE Trans. Plasma Sci.* 47(11) 4909

[24] Norberg S A, Johnsen E and Kushner M J 2015 *J. Appl. Phys.* 118 013301

[25] Li C, Pei X and Lu X 2017 *J. Appl. Phys.* 121 203305

[26] Darny T, Pouvesle J M, Puech V, Douat C, Dozias S and Robert E 2017 *Plasma Sources Sci. Technol.* 26 045008

[27] Sobota A, Guaitella O and Garcia-Caurel E 2013 *J. Phys. D: Appl. Phys.* 46 5

[28] Damany X, Pasquiersa S, Blin-Simiand N, Bauville G, Bournonville B, Fleury M, Jeanney P and Santos Sousa J 2016 *Eur. Phys. J. Appl. Phys.* 75 24713

[29] Brandenburg R 2017 *Plasma Sources Sci. Technol.* 26 053001

[30] Marinov D, Braithwaite N S J 2014 Plasma Sources Sci. Tech. 23(6) 062005

[31] Hofmann S, Van Gessel A F H, Verreycken T and Bruggeman P 2011 Plasma Sources Sci. Tech. 20(6) 065010

[32] Hofmann S, van Gils K, van der Linden S, Iseni S and Bruggeman P 2014 European Phys. J. D 68(3) 56

[33] Golda J, Kogelheide F, Awakowicz P and Gathen V S Von Der 2019 Plasma Sources Sci. Tech. 28 095023

[34] Stoffels E, Sladek R E J, Kieft I E, Kersten H and Wiese R 2004 *Plasma Phys. Control. Fusion* 46 B167–B177

[35] Teschner T, Bansemer R, Weltmann K D, Gerling T 2019 *Plasma* 2 348–359

[36] Maletić D, Puač N, Selaković N, Lazović S, Malović G, Đorđević A and Petrović Z Lj 2015 *Plasma Sources Sci. Technol*. 24 (2) 025006

[37] Ohring M 1995 Engineering Materials Science (New York: Academic Press)

[38] MatWeb Material Property Data http://www.matweb.com/ (Accessed 1 Jul 2019)

[39] Malmberg C G and Maryott A A 1956 Dielectric constant of Water from 0° to 100° C *J. Res. Nat. Bureau Standards* 56 2641

[40] Engineering ToolBox, Dielectric Constants of common Liquids https://www.engineeringtoolbox.com/liquid-dielectric-constants-d_1263.html (Accessed 1 Jul 2019)

[41] Phelps A V and Petrovic Z Lj 1999 *Plasma Sources Sci. Technol*. 8 R21

[42] Panzner G, Egert B, Schmidt H P 1985 *Surface Science* 151(2–3), 400-408

[43] Bruggeman P, Iza F, Lauwers D and Gonzalvo YA 2010 *J. Phys. D: Appl. Phys.* 43(1) 012003

[44] Murakami T, Niemi K, Gans T, O'Connell D and Graham WG, 2012 *Plasma Sources Sci. Technol* 22(1) 015003

[45] Fang Z, Shao T, Yang J and Zhang C 2016 Discharge processes and an electrical model of atmospheric pressure plasma jets in argon. *Eur. Phys. J. D* 70 3

[46] Valdivia-Barrientos R, Pacheco-Sotelo J, Pacheco-Pacheco M, Benítez-Read J S and López-Callejas R 2006 *Plasma Sources Sci. Technol.* 15 237-245

[47] Fang Z, Ji S, Pan J, Shao T and Zhang C 2012 *IEEE Trans. On Plasma Sci.* 40(3) 883-891

[48] Maletić D 2018 Development and diagnostics of atmospheric plasma jet and application on biological samples *PhD Thesis* Belgrade: University of Belgrade

[49] Golubovskii Yu B, Maiorov V A, Behnke J, Behnke J F 2003 *J. Phys. D: Appl. Phys.* 36 39–49

[50] Liu S and Neiger M 2003 *J. Phys. D: Appl. Phys.* 36 3144

[51] Walsh J L, Iza F, Janson N B, Law VJ and KongM G 2010 *J. Phys. D: Appl. Phys.* 43 075201

[52] Brandenburg R, Navrátil Z, Jánský J, St'Ahel P, Trunec D and Wagner H E 2009 *J. Phys. D: Appl. Phys.* 42 085208

[53] Sobota A, Guaitella O and Rousseau A 2014 *Plasma Sources Sci. Technol.* 23 025016

[54] Darny T, Pouvesle J M, Fontane J, Joly L, Dozias S, Robert E 2017 *Plasma Sources Sci. Technol.* 26 105001

ACCEPTED

[55] Viegas P, Slikboer E, Obrusník A, Bonaventura Z, Sobota A, Garcia-Caurel E, Guaitella O and Bourdon A 2018 *Plasma Sources Sci. Technol.* 27 094002

[56] Simoncelli E, Stancampiano A, Boselli M, Gherardi M and Colombo V 2019 *Plasma* 2 369–379

[57] Yue Y, Pei X, Gidon D, Wu F, Wu S and Lu X 2018 *Plasma Sources Sci. Technol.* 27 064001

[58] Gerling T, Brandenburg R, Wilke C and Weltmann K D 2017 *Eur. Phys. J. Appl. Phys.* 78 10801

[59] Pipa A V, Koskulics J, Brandenburg R and Hoder T 2012 *Rev. Sci. Instrum.* 83 115112

[60] Puač N, Petrović Z Lj, Radetić M and Djordjević A 2005 *Materials Science Forum* 494 291-296

ACCEPTED